RESEARCH ARTICLE

Computational repurposing of approved drugs targeting KRAS G12D and EGFR for colorectal cancer therapy

Walaa Ibraheem[1]*, Fatima Alsheikh[2,3], Abdulrahim A. Alzain[4], Bhoomendra A. Bhongade[1], Laila Ejaz[1], Hamnah Baig[5], Robert C. Robinson[2], Mohamed El-Tanani[1]

1 RAK College of Pharmacy, RAK Medical & Health Science University, RAK, UAE, **2** School of Biomolecular Science and Engineering (BSE), Vidyasirimedhi Institute of Science and Technology (VISTEC), Rayong, Thailand, **3** Division of Microbiology, Department of Pharmaceutics, Faculty of Pharmacy, University of Gezira, Gezira, Sudan, **4** Department of Pharmaceutical Chemistry, Faculty of Pharmacy, University of Gezira, Gezira, Sudan, **5** RAK College of Medicine, RAK Medical & Health Science University, RAK, UAE

* walaa.ibraheem@rakmhsu.ac.ae

Check for updates

OPEN ACCESS

Citation: Ibraheem W, Alsheikh F, Alzain AA, Bhongade BA, Ejaz L, Baig H, et al. (2026) Computational repurposing of approved drugs targeting KRAS G12D and EGFR for colorectal cancer therapy. PLoS One 21(1): e0338123. https://doi.org/10.1371/journal.pone.0338123

Editor: Khalid Raza, Jamia Millia Islamia Central University: Jamia Millia Islamia, INDIA

Received: June 3, 2025

Accepted: November 18, 2025

Published: January 28, 2026

Copyright: © 2026 Ibraheem et al. This is an open access article distributed under the terms of the Creative Commons Attribution License, which permits unrestricted use, distribution, and reproduction in any medium, provided the original author and source are credited.

Data availability statement: All relevant data are within the manuscript and its Supporting information files.

Funding: The author(s) received no specific funding for this work.

Abstract

Background/objectives

Colorectal cancer is characterized by various oncogenic mutations, with the KRAS ^{G12D} mutation being the most prevalent. The development of MRTX1133 has revitalized the KRAS direct targeting. However, colorectal cancer demonstrated intrinsic resistance to MRTX1133, primarily due to the feedback activation of the EGFR pathway. Combining KRAS ^{G12D} and EGFR inhibition has demonstrated improved treatment efficacy, highlighting the potential of dual-targeting approaches in colorectal cancer therapy. This study employs CADD tools to identify approved drugs capable of dual targeting KRAS ^{G12D} and EGFR.

Methods

A library of 3,591 approved drugs was screened against KRAS ^{G12D} using high-throughput virtual screening (HTVs), standard precision (SP) and extra precision (XP) Glide docking modules. The top-ranking compounds were then docked into the EGFR binding pocket using XP mode, and docking scores were calculated. Further refinement of binding affinities was performed using Molecular Mechanics with Generalized Born and Surface Area Solvation (MM-GBSA) and Molecular Dynamics (MD) simulations.

Results

A total of 25 drugs showed better affinity to KRAS ^{G12D} than MRTX1133 (−9.18 kcal/mol). Among them, six drugs: Reproterol, Macimorelin, Nebivolol, Nadolol,

Competing interests: The authors have declared that no competing interests exist.

Antrafenine, and Carteolol, displayed docking scores between −7.186 and −8.864 kcal/mol against EGFR, compared to the reference ligand Erlotinib (−9.669 kcal/mol). Subsequent MM-GBSA and MD identified Carteolol, an FDA-approved beta blocker, as the most promising candidate, showing stable and reliable binding with KRAS ^{G12D} and relatively stable interactions with EGFR.

Conclusions

This *in silico* study predicts Carteolol as a potential dual-targeting therapeutic agent, requiring biochemical and cellular validation before clinical relevance can be established.

1. Introduction

Kirsten rat sarcoma viral oncogene (KRAS) plays a significant role in tumor initiation and progression in a broad spectrum of human cancers. They account for >80% of all RAS mutations and are implicated in 20% of all human malignancies. The incidence of KRAS mutations is particularly high in colorectal cancer (CRC), occurring in 35–40% of CRC cases. Especially, the KRAS ^{G12D} mutation is a more dominant variant found in 12% of CRC cases and is significantly associated with a high risk of metastasis and a poor prognosis [1–3].

KRAS is stimulated by extracellular growth signals mediated by the epidermal growth factor receptor (EGFR) family. This growth signaling allows KRAS to shuttle between binding with guanosine-5′-triphosphate (GTP) in an 'on' state and with guanosine-5′-diphosphate (GDP) in an 'off' state. Mutations in KRAS alter the dynamics of this cycle, resulting in hyperactive KRAS, which constitutively activates three major pathways downstream: the mitogen-activated protein (MAP) kinase pathway, the PI3K/AKT/mTOR (PAM) pathway, and the tumor invasion and metastasis-inducing protein 1 (TIAM1–RAC) and RAS-related protein (RAL) pathways. This uncontrolled signaling results in increased proliferation, decreased apoptosis, and increased angiogenesis, contributing to oncogenesis. Therefore, directly targeting mutant KRAS could serve as an effective therapeutic strategy [1,2,4,5].

Targeting of KRAS has been considered quite challenging. Preliminary studies of the KRAS proteins revealed that they lack a hydrophobic binding cavity other than the GTP/GDP binding pocket. However, GTP is naturally abundant within cells and designing effective nucleotide-competitive inhibitors presents a significant challenge. Furthermore, targeting the KRAS upstream or downstream effectors has either failed to produce desired results or led to significant adverse effects. A breakthrough in the field occurred in 2013 when advancements in understanding KRAS biology led to the identification of the first KRAS ^{G12C} inhibitor [2].

The identification of a new allosteric site within KRAS ^{G12C} has led to the development of covalent inhibitors targeting the reactive Cys12 in the KRAS^{G12C} mutant through structure-based design. However, the G12D mutation is the most common mutational event in KRAS, and only a small percentage of patients experience

positive outcomes from G12C-targeted therapy. Nevertheless, the development of specific KRAS ^{G12C} inhibitors revealed that the allosteric site in all KRAS proteins is a valid target for designing selective KRAS ^{G12D} inhibitors. In 2021, a selective noncovalent KRAS ^{G12D} inhibitor named MRTX1133 was developed, and preclinical studies indicate that it has the potential to revolutionize the approach to treating KRAS ^{G12D} -driven cancer, potentially reshaping the current therapeutic strategies [3,6–9]. Despite MRTX1133 being an effective inhibitor of KRAS ^{G12D} and demonstrating a cytotoxic effect on KRAS ^{G12D} -mutated cancer cells, a recent report concluded that KRAS ^{G12D} -mutated colorectal cancer cells exhibit a reduced sensitivity **to** MRTX1133, resulting in a weaker therapeutic response. This study revealed that feedback activation of the EGFR/wild-type RAS pathway reduces the effectiveness of KRAS ^{G12D} inhibitor therapy in CRC. Notably, wild isoforms of RAS, rather than oncogenic KRAS, trigger downstream signaling of the activated EGFR, resulting in a rebound reactivation and reduced MRTX1133 efficacy. Fortunately, the inhibition of this pathway with kinase inhibitors such as erlotinib blocked EGFR/wild-type RAS signaling and sensitized cells to MRTX1133 [10].

Drug repurposing emphasizes on identifying new therapeutic uses for existing approved and marketed drugs. Drugs that have already undergone clinical trials are proven safe with well-known pharmacokinetic, pharmacodynamic, and toxicity profiles, allowing researchers to explore their broader therapeutic potential. Compared to the 12–13 years and 2–3 billion USD needed to bring a new drug from bench to market, repurposing affords a faster and more affordable alternative, saving both cost and time by approximately 30% [11]. Moreover, the integration of computational approaches during the initial stages of drug discovery has proven to be invaluable. These approaches are now frequently employed at different phases of the drug development process, such as hit recognition and lead optimization. Virtual screening enables the narrowing of a vast array of compounds for experimental testing and the identification of promising drug candidates. Molecular docking is widely utilized in virtual screening, especially when the 3D structure of a protein is known. Moreover, molecular dynamics (MD) has emerged as a computational tool for exploring the flexibility and dynamics of drug–target interactions, revolutionizing the field of computer-aided drug design (CADD) [12–14]. Together, drug repurposing and advanced computational methods expedite the development pipeline, offering a cost-effective and time-saving pathway to identify effective therapeutic solutions [15].

This study utilizes computational methods to explore the repurposing potential of existing drugs to concurrently target KRAS ^{G12D} and EGFR. This dual-targeting strategy is intended to circumvent resistance and enhance the therapeutic efficacy of KRAS ^{G12D} -directed treatments.

2. Materials and methods

2.1. Computational resources

Maestro v 12.8 of the Schrodinger suite was used in this study.

2.2. Preparation of proteins and ligands

The three-dimensional (3D) structures of KRAS ^{G12D} (PDB ID: 7RPZ) and EGFR tyrosine kinase (PDB ID: 1M17) were retrieved from the Protein Data Bank (https://www.rcsb.org/structure). The two proteins were then prepared via the protein preparation wizard tool Maestro, which refines and optimizes the protein structures. The proteins were subsequently minimized via the OPLS3e force field [16,17].

The binding cavities of the proteins were defined around the co-crystallised ligands MRTX1133 and Erlotinib bound to the protein via the Receptor Grid Generation tool of Maestro. The coordinates of the ligands with the protein were used to create a 3D grid with precise dimensions, representing the receptor's active area [18].

A library of 3,591 approved drugs was obtained from the ChEMBL library (https://www.ebi.ac.uk/chembl/). During this process, Epik was employed to generate the most probable protonation and tautomeric states at physiological pH (7.0 ± 2.0). Subsequently, all compounds were energy minimized using the OPLS3e force field to generate low-energy conformers to ensure that the compound structures were acceptable for further computational work [19].

2.3. Molecular docking and MM-GBSA calculations

The prepared library served as an input for a multistage virtual screening to identify potential dual inhibitors for KRAS ^{G12D} and EGFR. Initially, the library was screened against KRAS G12D, and ligands were shortlisted based on their binding strength to the receptor, represented by the Glide score (G score). This process involved sequential docking steps via the Glide module. High-throughput virtual screening (HTVS) is used for quick and initial screening, followed by standard perception (SP) and extra precision (XP), which provides the highest accuracy. Default parameters were employed for the docking process, and the results were analyzed based on the G-scores [20–22].

Compounds that achieved high docking scores were further docked into the binding pocket of EGFR, and their docking score were calculated. The docking protocol was validated by redocking the native co-crystallized inhibitors into the prepared active sites of KRAS ^{G12D} and EGFR. In both cases, the re-docked poses closely reproduced the binding orientations observed in the co-crystallized structures, with root mean square deviation (RMSD) values of 2.06 Å and 1.09 Å, respectively (Fig 1).

The docking poses of the shortlisted compounds were then used to calculate their MM-GBSA binding free energy via the Prime tool of Maestro. MM-GBSA is a rescoring method that demonstrates a strong correlation between predicted and observed activity [23–25]. The binding free energy was calculated via the following equation [24]:

$$\Delta G\ \text{bind} = G\ \text{complex} - (G\ \text{protein} + G\ \text{ligand})$$

Where:

ΔG bind = binding free energy

G complex = free energy of the complex

G protein = free energy of the target protein

G ligand = free energy of the ligand.

The calculations applied the VSGB implicit solvation model and the OPLS3e force field, as integrated into the Schrödinger Prime module. The VSGB model approximates solvation effects without explicitly including solvent molecules, and the calculations were performed in an implicit solvent environment, not in vacuum. Additionally, entropy contributions were omitted, which is a common simplification in MM-GBSA workflows to reduce computational cost while maintaining reliable relative binding energy estimates [26].

2.4. Molecular dynamics (MD) simulations

The Glide XP docking output files were input for MD simulations conducted using the GROMACS 2024.4 software package. Ligand topologies were generated using the SwissParam server, while protein parameters were generated using the

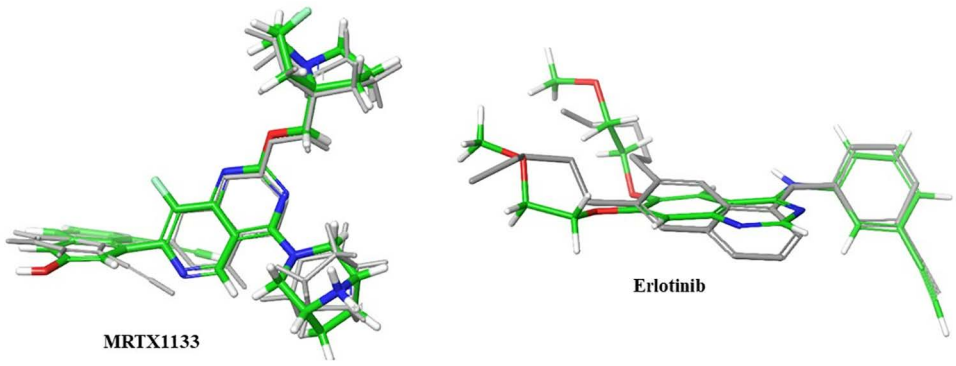


Fig 1. The 3D structures of the redocked MRTX1133 and Erlotinib(Grey)superimposed on the co-crystalized structures (Green).

https://doi.org/10.1371/journal.pone.0338123.g001

OPLS-AA/L force field and TIP3P water model within GROMACS [27]. A triclinic simulation box was created around the protein-ligand complexes using the gmx editconf module. For EGFR, the box was set to an orthorhombic shape, and the protein-drug complex was positioned at the center of the 11.4 x 8.6 x 7.2 nm box. The KRAS ^{G12D} protein-drug complex was positioned at the center of a cubic box with a 6 nm distance. Water molecules were added to fully solvate the systems, along with Na ions to neutralize the system, and pairs of Na and Cl ions were added to achieve a 0.1 M salt concentration. Following box preparation, the system underwent energy minimization using the steepest descent algorithm. Subsequently, NVT (constant number of particles, volume, and temperature) and NPT (constant number of particles, pressure, and temperature) equilibration runs were performed for 100 ps to achieve a stable system at the desired temperature and pressure. The stability of the complexes was assessed using root means square deviation (RMSD), root mean square fluctuation (RMSF), and radius of gyration (Rg).

2.5. In silico ADME prediction

The physicochemical characteristics of the highest-scoring ligands were analysed using the pkCSM web server, accessible at https://biosig.unimelb.edu.au/pkcsm/. This tool facilitates the prediction of ADME parameters to evaluate the drug-likeness of the compounds.

3. Results and discussion

The emergence of targeted therapies, such as the selective inhibitor MRTX1133, has revolutionized the treatment of KRAS ^{G12D}-mutated cancers [7]. While this compound has demonstrated cytotoxic effects on KRAS ^{G12D}-mutated cancer cells, recent reports revealed that CRC cells harbouring this mutation often display diminished responsiveness to MRTX1133 [28]. The reduced efficacy has been attributed to feedback activation of the EGFR/wild-type RAS pathway. However, the inhibition of activated EGFR has been shown to suppress this compensatory signalling, thereby increasing sensitivity to MRTX1133 [10]. Given these challenges, our study aims to employ CADD to assess the potential of repurposing approved drugs to inhibit both the KRAS ^{G12D} and EGFR proteins. By employing CADD, we can efficiently screen a library of approved drugs to identify candidates that may simultaneously target both the KRAS ^{G12D} and the EGFR. This approach enhances the therapeutic efficacy and overcomes the limitations posed by feedback mechanisms in CRC treatment.

The active sites for KRAS and EGFR were determined using the bound ligands to both proteins. The active site of KRAS (PDB ID: 7RPZ) bound to MRTX1133 was validated using the SiteMap of the Schrodinger suite which showed site-1 residues were consistent with the interacting residues of MRTX1133 bound to KRAS (S1 Table, supplementary file)

As represented in Fig 2, the workflow involved two rounds of docking. In the 1st round, a library of 3,591 approved drugs was screened against KRAS ^{G12D}. Consecutive docking steps employing the Glide module were implemented to filter the most promising candidate from this library and to analyze the nature of interactions between the target and ligands. Regardless of its limitation in accounting for the flexibility of receptors, docking remains a valid tool for providing preliminary insights. Preliminary screening via Glide's HTVS mode revealed that 634 compounds presented docking scores of −7 kcal/mol or lower. These compounds were then subjected to SP docking, and the top 100 compounds with SP scores < −8.2 kcal/mol were selected for further refinement. Extra Precision (XP) docking was subsequently performed on this subset. To prioritize compounds with superior predicted binding affinities, we applied a selection criterion based on outperforming the reference ligand MRTX1133, which had an XP docking score of −9.18 kcal/mol. Accordingly, compounds with lower XP scores were shortlisted. This resulted in 25 top-ranking compounds with XP scores ranging from −9.202 to −10.866 kcal/mol, all demonstrating stronger predicted binding than the reference. The top-ranked were subsequently selected for a second round of XP docking against the EGFR. The EGFR docking results indicated that six approved drugs, namely Reproterol, Macimorelin, Nebivolol, Nadolol, Antrafenine and Carteolol, achieved docking scores ranging between −7.186 to −8. 864 kcal/mol. In comparison, the reference ligand Erlotinib exhibited a docking score of −9.669 kcal/mol.

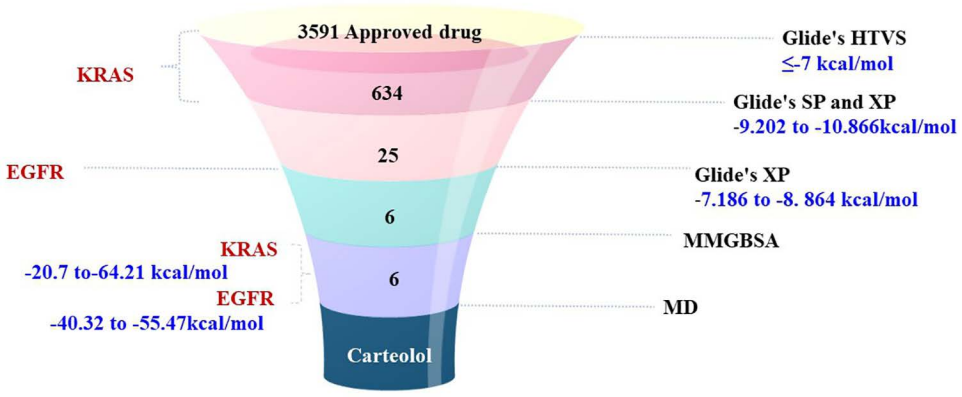


Fig 2. Summary of the study workflow.

https://doi.org/10.1371/journal.pone.0338123.g002

The strength of the binding affinity for the top six drugs was evaluated by calculating the binding free energy. The obtained dGbind values ranged from-20.7 to-64.21 kcal/mol for KRAS ^{G12D} and −40.32 to –55.47 kcal/mol for EGFR (Table 1). The reference ligands MRTX1133 and Erlotinib exhibited an MM-GBSA value of −27.15 and −65.58 kcal/mol, respectively (Table 1). These calculations were performed without including entropy contributions, a common simplification in MM-GBSA workflows aimed at reducing computational cost. However, this omission represents a notable limitation, especially when interpreting absolute binding energies, which may lack accuracy in the absence of entropic terms. Despite this, relative binding energy comparisons remain robust and continue to provide valuable insights into ligand ranking and binding strength. less accurate without entropic terms. Relative binding energy comparisons remain reliable under this approach and continue to offer meaningful insights into ligand ranking and binding strength.

Notably, our primary objective is not to identify candidates with superior EGFR binding compared to Erlotinib, but rather to identify compounds that exhibit strong affinity for KRAS ^{G12D} while also modulating EGFR. This dual-targeting strategy aims to address resistance mechanisms often encountered in colorectal cancer. Therefore, these compounds were taken forward for detailed structural and binding interaction analysis.

Interestingly, among the shortlisted compounds, three beta-adrenoceptor blockers (Nebivolol, Nadolol and Carteolol) and one short-acting agonist (Reproterol) were identified. Notably, the six shortlisted compounds share common structural features, including a protonated primary (as in the case of Macimorelin) or secondary amine group, a bicyclic nucleus, and alkyl substituents. These structural elements contribute to the formation of an extensive hydrophobic interface, which has the potential to serve as an effective framework for developing KRAS ^{G12D} inhibitors [29].

Table 1. The docking and MM/GBSA result for the shortlisted drugs and reference ligands.

Drug name	Chembl ID	XP Gscore KRAS^{G12D}	XP Gscore EGFR	MMGBSA KRAS^{G12D}	MMGBSA EGFR
Reproterol	CHEMBL1095607	−7.935	−8.864	−37.93	−40.81
Nebivolol	CHEMBL434394	−10.006	−8.123	−29	−46.32
Nadolol	CHEMBL521606	−10.989	−7.816	−64.21	−49.65
Macimorelin	CHEMBL278623	−9.49	−7.638	−15.74	−49.2
Carteolol	CHEMBL839	−9.372	−7.185	−57.95	−49.26
Antrafenine	CHEMBL345524	−9.101	−7.856	−20.7	−55.47
Erlotinib			−9.669		−65.58
MRTX1133		−9.18		−27.15	

https://doi.org/10.1371/journal.pone.0338123.t001

It has been reported that the key amino acids contributing to the stability of KRAS ^{G12D}, in descending order of significance, are: Asp69, His95, Met72, Gln99, Arg68, Tyr96, Tyr64, Gly60, Asp12, and Val9 [29]. As shown in Fig 2 and Table 2, all the shortlisted compounds, except for Macimorelin and Antrafenine, exhibited a shared interaction with Arg68. Macimorelin, however, formed a hydrogen bond with Tyr96 and a pi-pi stacking interaction with His95, mirroring the interactions observed in Reproterol. In reproterol, though, the interaction with His95 was through a hydrogen bond. Antrafenine, Carteolol and Nadolol establish a structured hydrogen bond network. This network enables the ligands to effectively connect the lipophilic and polar regions of the switch II pocket. This network is established through a water bridge, involving the conserved water molecules within the binding site. In this interaction, the hydroxyl group of Thr58 and the carbonyl oxygen of Gly10 function as hydrogen acceptors, while the amine groups of the ligands serve as hydrogen donors. Nadolol also

Table 2. The intermolecular interactions of the shortlisted drugs and MRTX1133 with KRAS ^{G12D}.

Drug name	H-bond	Water bridge	π-cation	π-π stacking	Hydrophobic interaction	Others
Reproterol	H_2O, Arg68, Hid 95, Tyr96				Val9. Ala11, Val14, Pro34, Ala59, Phe78, Met72, Tyr64, Tyr96, Ile100, Val103	Polar: Ser17, Thr35, Thr58, Hid95, Gln99
						Charged negative: Asp69, Glu62, Glu63, Asp92
						Charged positive: Arg68, Lys88Arg102
						Gly10
Nebivolol	Arg68				Val9. Ala11, Val14, Ala59, Phe78, Met72, Tyr64, Tyr96, Ile100, Val103	Polar: Thr58, Gln61 Hid95, Gln99
						Charged negative: Asp12, Asp69, Glu62, Glu63, Asp92
						Charged positive: Arg68, Lys88 Arg102
						Gly10, Gly60
Nadolol	H_2O Arg68, Asp69, Arg102	Gly10, Thr58			Val9. Ala11, Ala59, Met72, Tyr64, Tyr96, Ile100, Val103	Polar: Thr58, Gln61, Gln99
						Charged negative: Asp12, Asp69, Glu62, Glu63.
						Charged positive Lys16 Arg68Arg102
						Gly10, Gly60
Macimorelin	Tyr96			Hid95	Val9. Ala11, Ala59, Phe78, Met72, Tyr64, Tyr96, Ile100, Val103	Polar: Thr58, Gln61 Hid95, Gln99
						Charged negative: Asp12, Asp69, Glu62, Glu63.
						Charged positive Lys16, Lys88Arg102
						Gly10, Gly60
Carteolol	Arg68	Gly10, Thr58, Ala59, Gln61, Arg68			Val9. Ala11, Ala59, Phe78, Met72, Tyr64, Tyr96, Ile100, Val103	Polar: Thr58, Gln61, Gln99
						Charged negative: Asp12, Glu62, Glu63, Asp69.
						Charged positive Lys16, Arg68, Arg102
						Gly10, Gly60
Antrafenine		Gly10, Thr58	Hid95		Val9. Ala11, Met72, Tyr64, Tyr96, Ile100, Val103	Polar: Thr58, Hid95, Gln99
						Charged negative: Glu62, Glu63, Asp69, Asp92
						Charged positive Arg68, Lys88, Arg102
						Gly10
MRTX1133	Asp12, Glu62		Hid95	Tyr96	Val9. Ala11, Ala59, Phe78, Met72, Tyr64, Tyr96, Ile100, Val103	Polar: Ser65, Gln61, Hid95, Gln99
						Charged negative: Asp12, Asp69, Glu62, Glu63
						Charged positive: Lys16, Arg68, Arg102

https://doi.org/10.1371/journal.pone.0338123.t002

forms hydrogen bonds with Asp69 and Arg102. Prior research suggests that inhibitors forming such networks are associated with a stronger inhibitory effect [9]. Conversely, MRTX1133 is stabilized in the binding pocket through hydrogen bonds with Asp12 and Glu62, as well as pi–pi and pi-cation interactions with Tyr96 and His95, respectively (Fig 3 and Table 2).

Furthermore, the structural attributes of the selected compounds facilitate the formation of a robust hydrogen bond network within EGFR's ATP binding pocket. A sustained hydrogen bond with Met769 was noted, along with an ionic interaction between the cationic amino groups of these compounds and the carboxylic acid side chain of Asp831. Previous research has reported that the interaction with Asp831 can enhance EGFR inhibition by 50-fold [30]. It is worth mentioning that nebivolol, while not interacting with Met769, did interact with Cys773. This interaction was pivotal in the creation of irreversible EGFR inhibitors, which exhibited significant anti-tumor activity. Effects in both in vitro and in vivo investigations, all while maintaining minimal cytotoxicity [9]. Moreover, Antrafenine, Carteolol, Nadolol, and Nebivolol exhibited additional interactions with Phe699. Nebivolol and Antrafenine also showed interactions with Lys721. Nadolol and Macimorelin interacted with a water molecule in the binding site, while Macimorelin and Nebivolol interacted with Arg817. Reproterol and Nebivolol uniquely interacted with Glu738 and Thr830, respectively. Erlotinib formed hydrogen bonds with Met769 and water molecules in the EGFR binding site (Fig 4 and Table 3).

The flexibility of the receptor is crucial for reliably predicting drug binding affinity, thermodynamic properties, and kinetic behavior. Integrating docking studies with MD simulations can therefore improve the screening process and facilitate the identification of novel lead compounds [31]. Nadolol and Carteolol were identified as promising candidates, demonstrating the highest docking scores with KRAS ^{G12D} and acceptable scores with EGFR. The compounds were then analyzed using 100 ns molecular dynamics (MD) simulations to assess their binding stability. Key parameters analyzed included the root mean square deviation (RMSD), the root mean square fluctuation (RMSF), and the radius of gyration of the ligand. The RMSD is used to quantify the average movement of a selection of atoms in a specific

frame compared to a reference frame. Analyzing RMSD provides valuable insights into a protein's structural conformation throughout the simulation, where lower values and fewer deviations signify higher stability. The RMSD values were calculated and displayed on a graph, where the x-axis represents simulation time ranging from 0 to 100 ns, and the y-axis shows RMSD values in nanometers (nm). The RMSD statistics were presented in S2 and S3 Table in the supplementary files. The RMSD plot for the KRAS ^{G12D} protein revealed that all three ligands, Nadolol, Carteolol, and MRTX1133 maintained a stable interaction with the KRAS ^{G12D} protein throughout the simulation, as evidenced by the low RMSD values. The curves of Carteolol (blue) and Nadolol (orange) are closely aligned, displaying a stable pattern with negligible fluctuations, ranging between 0.06 nm and 0.16 nm and an average RMSD of 0.124 nm. In contrast, the reference ligand (black) exhibited slightly higher RMSD values ranging between 0.059 nm and 0.21 nm, and an average RMSD of 0.156 nm, indicating greater fluctuations compared to Carteolol and Nadolol, suggesting that MRTX1133 leads to a less stable conformation of the KRAS ^{G12D} protein (Fig 5). To further illustrate the conformational evolution of the ligand throughout the simulation, snapshots at 0 ns, 50 ns, and 100 ns were represented to capture the initial, intermediate, and final binding pose (Fig 6). The visual progression highlights the dynamic nature of ligand–receptor interactions within the binding pocket. Initially, carteolol was stabilized through its interaction with Tyr96. As the simulation progressed, this interaction was replaced by new contacts with Gln61 and Glu62, which ultimately stabilized the ligand in its final binding conformation. Similarly, nadolol exhibited a shift in its binding profile: it was first stabilized by Asp69, Glu63, and Arg102, followed by a transition to Glu62, and eventually settled into a conformation supported by interactions with both Glu62 and Tyr64.

In Fig 7, the RMSD analysis of the EGFR-ligand complexes highlights distinct stability patterns among Erlotinib, Carteolol, and Nadolol. The EGFR with Erlotinib in black displayed a stable pattern with minimal fluctuations, maintaining an average RMSD of 0.34 nm. In contrast, Carteolol in blue exhibited an initial equilibrium state around 0.2 nm for the first 68 ns, followed by fluctuations lasting for 8 ns, after which the system restabilized at approximately 0.7 nm until the end of

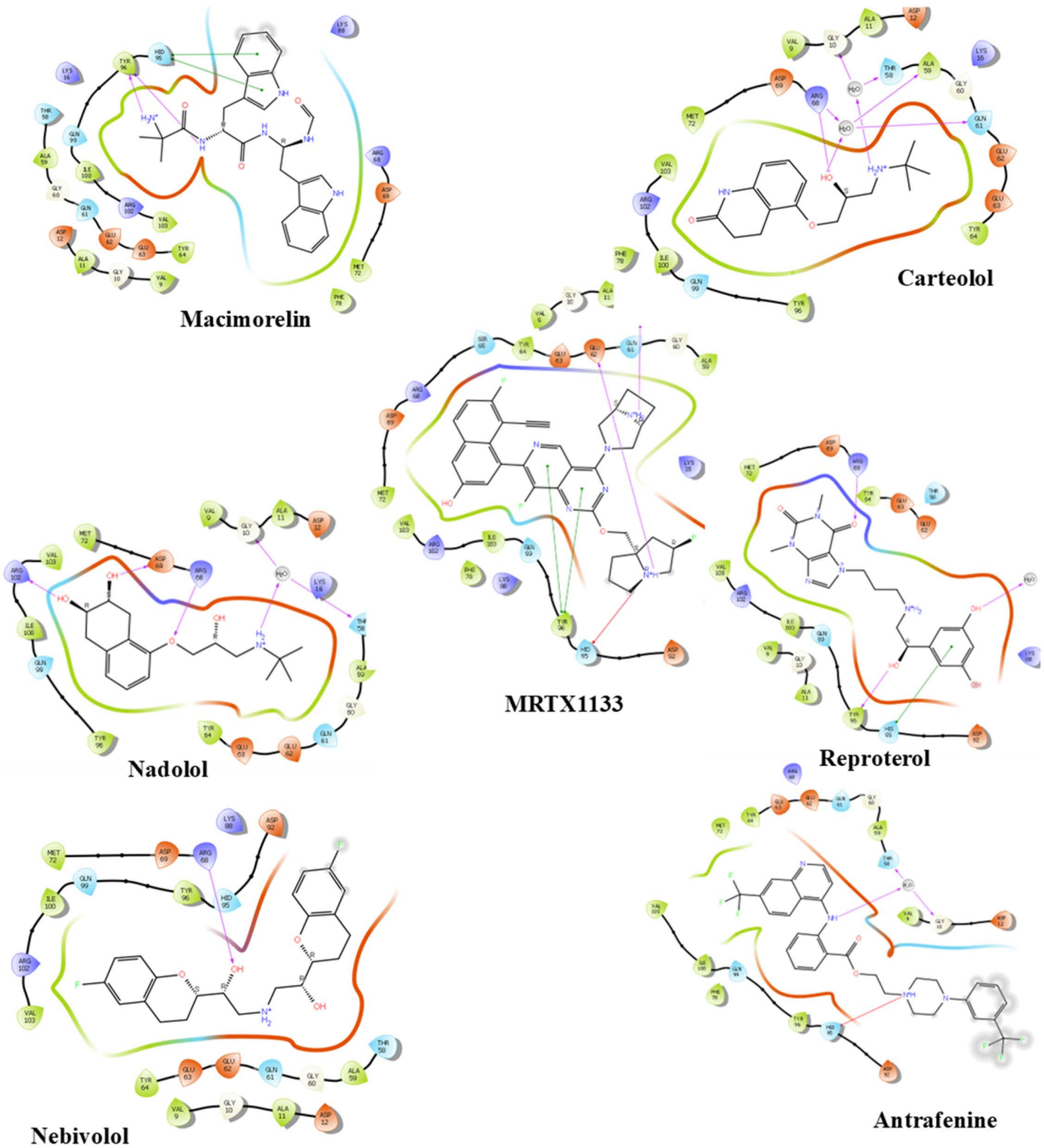


Fig 3. The two-dimensional (2D) interactions of the shortlisted drugs and MRTX1133 with KRAS $^{G}12^{D}$ (PDB ID: 7RPZ). The hydrogen bond interactions with residues are represented in a purple arrow, while a red-blue arrow represents the salt bridge, hydrophobic interactions are represented with green residues, polar interactions with faint blue residues, positive interactions with dark blue residues and negative interactions with red residues.

https://doi.org/10.1371/journal.pone.0338123.g003

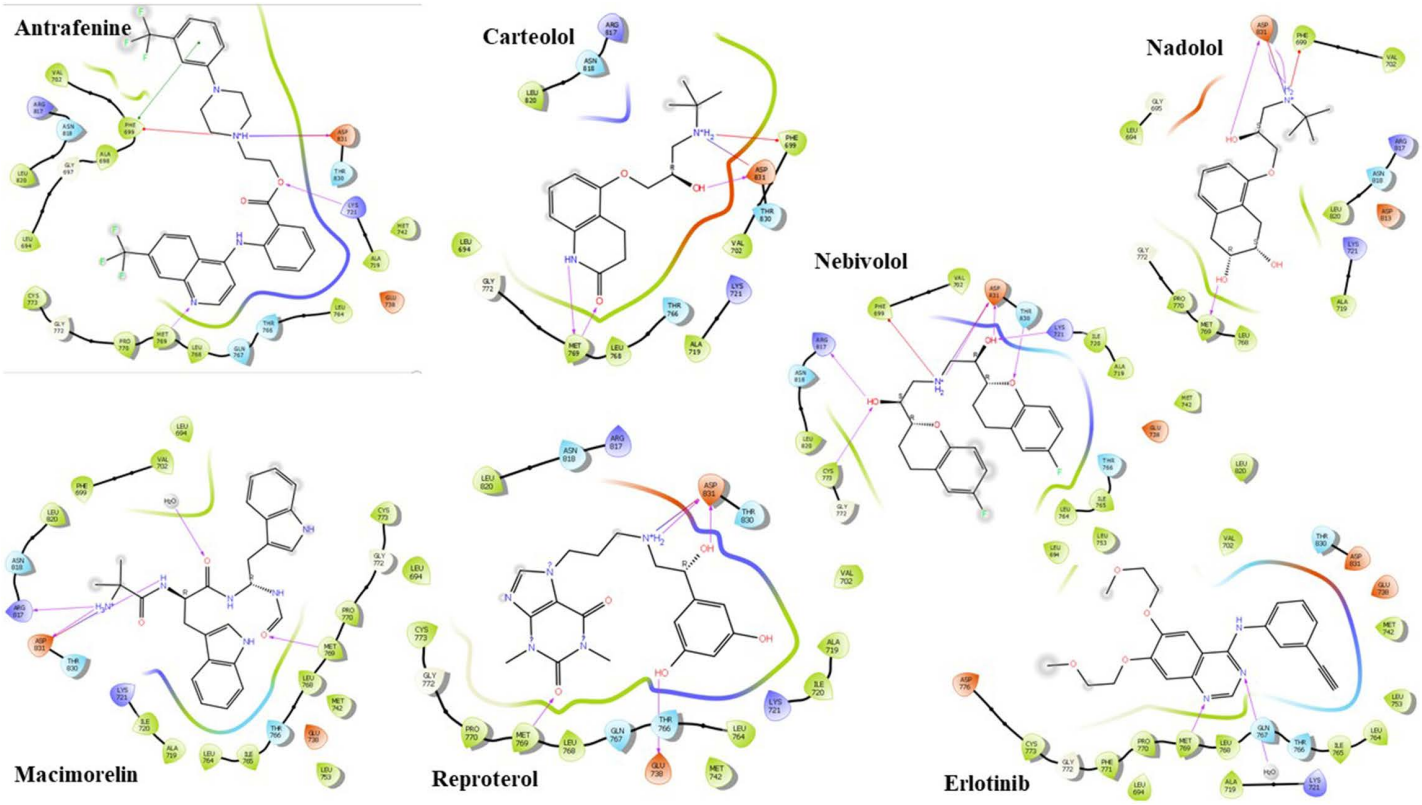


Fig 4. The two-dimensional (2D) interactions of the shortlisted drugs and Erlotinib with EGFR (PDB ID: 1M17). The hydrogen bond interactions with residues are represented in a purple arrow, while a red-blue arrow represents the salt bridge, hydrophobic interactions are represented with green residues, polar interactions with faint blue residues, positive interactions with dark blue residues and negative interactions with red residues.

https://doi.org/10.1371/journal.pone.0338123.g004

the simulation. This suggests Carteolol experiences some instability and conformational changes within the EGFR binding pocket.

As shown in Fig 8, Carteolol, initially stabilized through hydrogen bonds with ASP 831 and LYS 721, maintaining low RMSD for the first 65 ns. Following this phase, the ligand undergoes a structural shift, increasing RMSD. However, the ligand subsequently establishes new interactions with MET 769 and LEU 694, leading to re-stabilization within the binding pocket. This dynamic behavior indicates the ligand can adapt and optimize its binding interactions over time. On the other hand, Nadolol (orange) stabilized within the first 5 ns, but maintained a higher RMSD of 1 nm, which is significantly greater than the other two ligands. This suggests greater conformational variability and possibly weaker binding interactions with the EGFR pocket (Fig 7). Consistent with this, the snapshots in Fig 8 reveal notable positional shifts of nadolol within the binding site over time, reflecting its dynamic and less stable engagement with key residues.

Further analysis of MD trajectories using the Visual Molecular Dynamics (VMD) tool verified that Erlotinib and Carteolol remained within the simulation box, supporting their continued interaction with the target protein (S1 Video). Overall, Erlotinib exhibits the most favorable binding stability, followed by Carteolol, which demonstrates dynamic interaction characteristics, whereas Nadolol's elevated RMSD suggests less stable binding behavior.

To evaluate the stability of amino acid residues, we conducted RMSF analysis; a statistical tool that quantifies the extent of residue movement throughout a simulation. This analysis helps identify protein regions exhibiting significant fluctuations. The RMSF plot for the KRAS ^{G12D} and EGFR, each bound to Carteolol, Nadolol, and reference

Table 3. The intermolecular interactions of the shortlisted drugs and Erlotinib with EGFR.

Drug name	H-bond	Salt bridge	π-π stacking	π-Cation	Hydrophobic interaction	Others
Reproterol	Asp831 Glu738, Met769	Asp831			Leu694, Val702, Ala719, Ile720, Met742, Leu764, Leu768, Met769, Pro770, Cys773 Leu820.	Polar: Thr766, Gln767, Asn818, Thr830
						Charged negative: Glu738, Asp831
						Charged positive: Lys721, Arg817
						Gly772
Nebivolol	Lys721, Cys773, Arg817, Asp831, Thr830	Asp831		Phe699	Leu694, Phe699, Val702, Ile720, Met742, Leu764, Ile765, Cys773 Leu820.	Polar: Thr766, Asn818, Thr830
						Charged negative: Glu738, Asp831
						Charged positive: Lys721, Arg817
						Gly772
Nadolol	H2O Met 769, Asp831	Asp831		Phe699	Leu694, Phe699, Val702, Ala719, Leu768, Met769, Leu820.	Polar: Thr766, Gln767, Thr830
						Charged negative: Asp831, Asp813
						Charged positive: Lys721, Arg817
						Gly695
Macimorelin	H2O Met 769, Asp831 Arg817	Asp831			Leu694, Phe699, Val702, Ala719, Met742, Leu753, Leu768, Met769, Cys773 Leu753, Leu764, Ile765 Leu820.	Polar: Thr766, Asn818, Thr830
						Charged negative: Asp776, Glu738, Asp831.
						Charged positive: Lys721, Arg817
						Gly772
Carteolol	Met 769, Asp831	Asp831	Phe699		Leu694, Phe699, Val702, Ala719, Leu768, Met769, Leu820.	Polar: Thr766, Thr830
						Charged negative: Asp831
						Charged positive: Lys721
						Gly772
Antrafenine	Met 769, Lys721	Asp831	Phe699	Asp831 Phe699	Leu694, Ala698, Phe699, Val702, Ala719, Met742, Leu753, Leu768, Met769, Pro770, Phe771, Cys773 Leu753, Leu764, Ile765 Leu820, Phe832.	Polar: Thr766, Gln767, Asn818, Thr830
						Charged negative: Asp831, Glu738
						Charged positive: Lys721, Arg817
						Glys697, Gly772
Erlotinib		Water, Met769			Leu694Val702, Ala719, Met742, Pro770, Cys773, Phe771Leu768, Met769, Leu753, Leu764, Ile765 Leu820,	Polar: Gln767, Thr766
						Charged negative: Asp831, Glu738, Asp776
						Charged positive: Lys721
						Gly772

https://doi.org/10.1371/journal.pone.0338123.t003

ligands, indicated that most residues displayed only slight fluctuations, with RMSF values remaining below 0.3 nm for KRAS ^{G12D} and 0.4 nm for EGFR. It is worth noting that the regions showing higher RMSF values were remote from the binding cavity, reflecting a well-preserved structure in the KRAS ^{G12D} and EGFR when bound to three ligands (Figs 9 and 10). Despite its higher RMSD, Nadolol's lower RMSF suggests that while the overall structure undergoes significant conformational changes, certain regions of the protein remain stable. This indicates that nadolol may stabilize specific areas of the protein, even as the complex undergoes broader structural changes throughout the simulation.

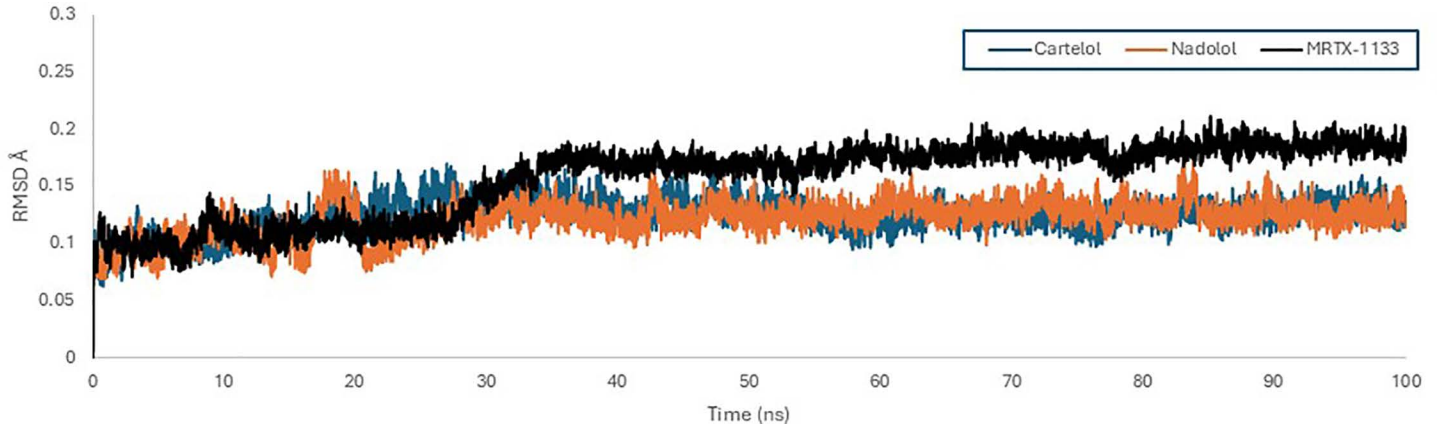


Fig 5. Root mean square deviation (RMSD) graphical record of KRAS $^{G}12^{D}$ (PDB ID: 7RPZ) with Carteolol (Blue), Nadolol (orange)and MRTX1133 (Black) over a 100 ns simulation time using GROMACS software.

https://doi.org/10.1371/journal.pone.0338123.g005

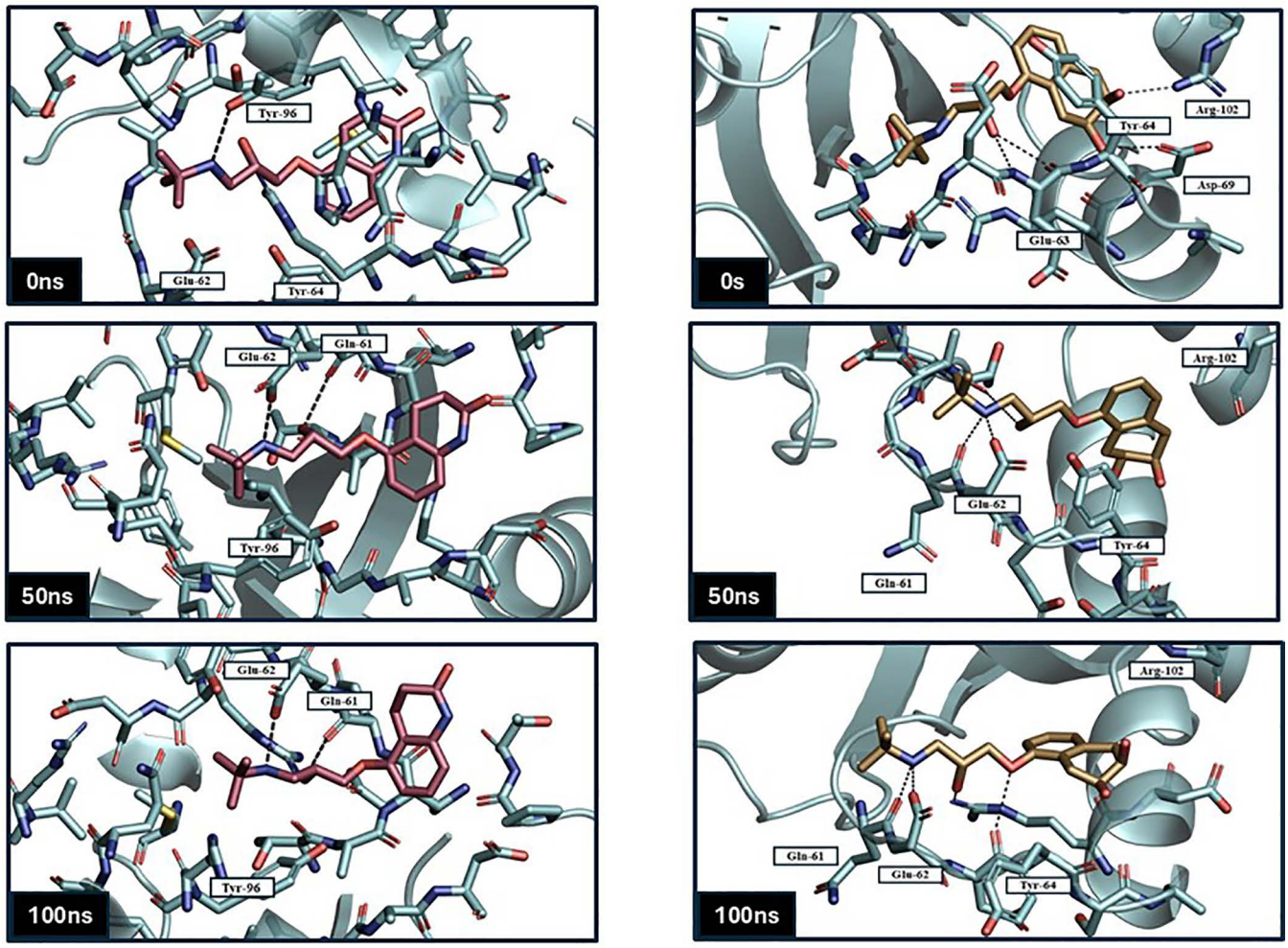


Fig 6. Representative snapshots of Carteolol (Red) and Nadolol (Sand)within KRAS $^{G}12^{D}$ binding pocket at 0 ns, 50 ns, and 100 ns during the molecular dynamics simulation over a 100 ns simulation time using GROMACS software.

https://doi.org/10.1371/journal.pone.0338123.g006

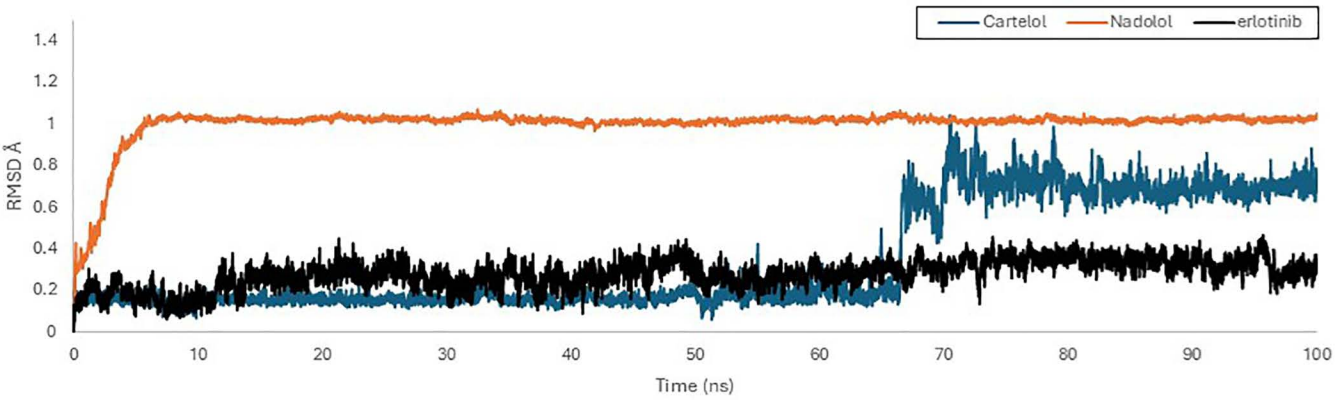


Fig 7. Root mean square deviation (RMSD) graphical record of EGFR (PDB ID: 1M17) with Carteolol (Blue), Nadolol (orange) and Erlotinib (Black) over a 100 ns simulation time using GROMACS software.

https://doi.org/10.1371/journal.pone.0338123.g007

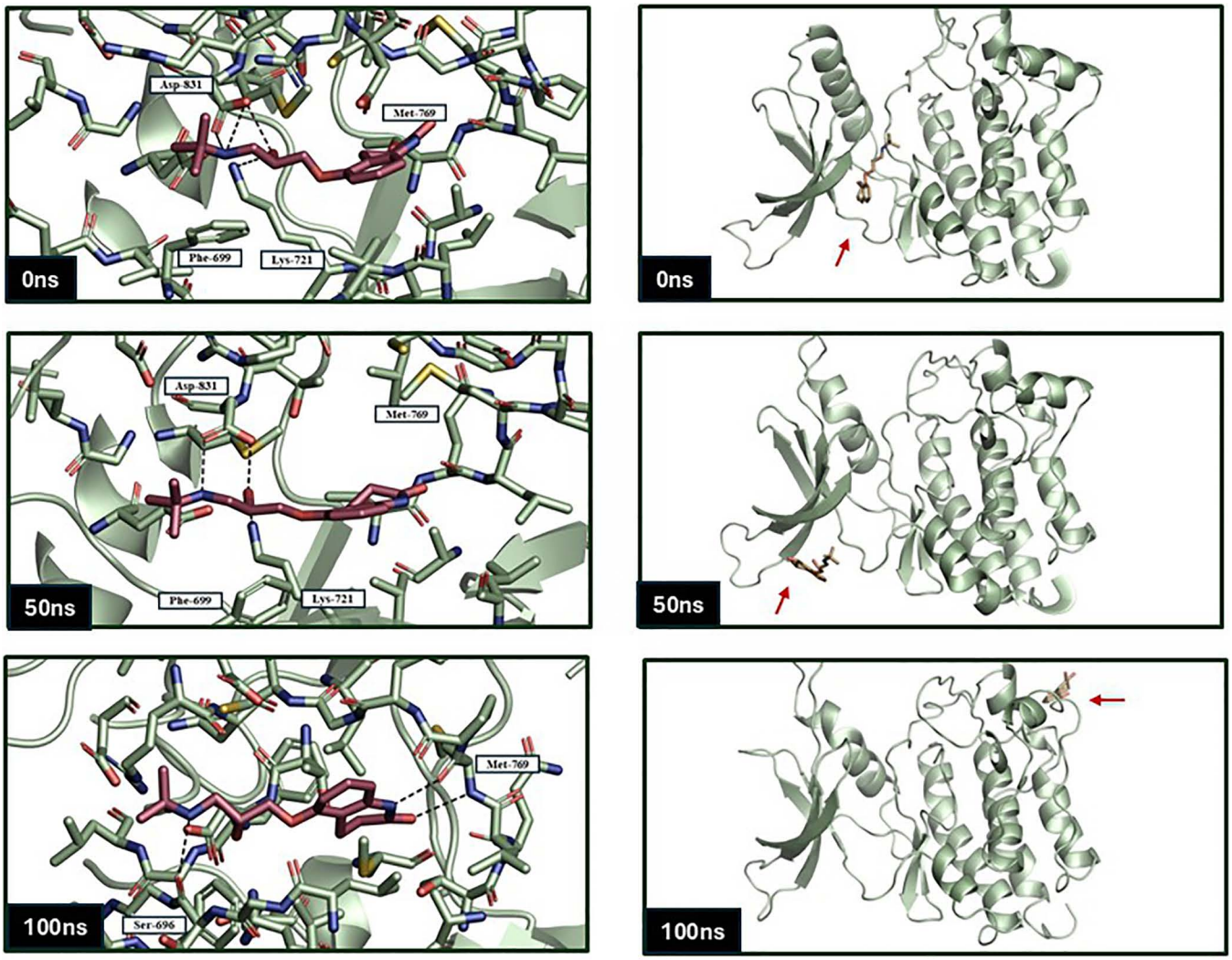


Fig 8. Representative snapshots of Carteolol (Red) and Nadolol (Sand) within the EGFR binding pocket at 0 ns, 50 ns, and 100 ns during the molecular dynamics simulation in EGFR over a 100 ns simulation time using GROMACS software.

https://doi.org/10.1371/journal.pone.0338123.g008

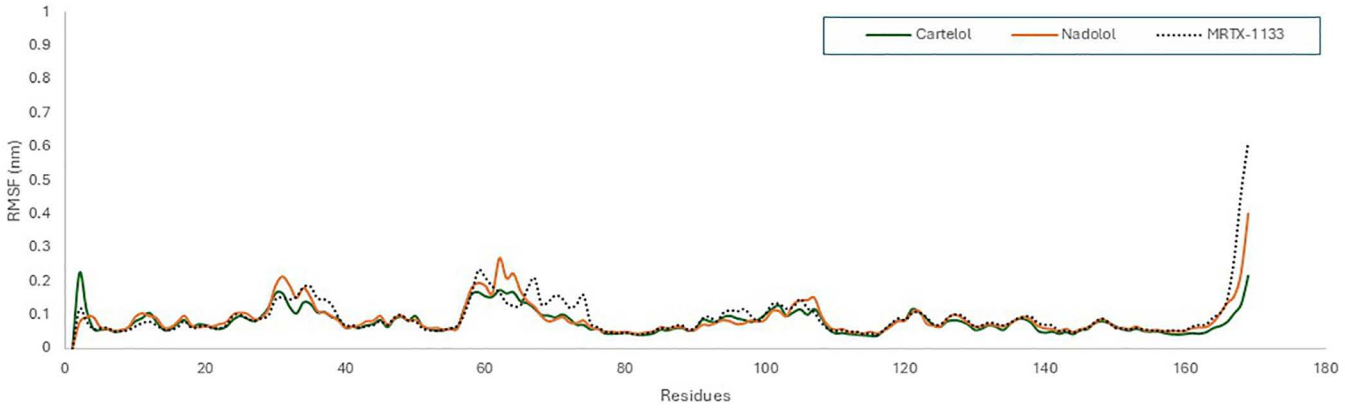


Fig 9. The root means square fluctuation RMSF profile of KRAS $^{G}12^{D}$ (PDB ID: 7RPZ) with Carteolol (green), Nadolol (orange)and MRTX1133 (Black) over 100 ns simulation time using GROMACs software.

https://doi.org/10.1371/journal.pone.0338123.g009

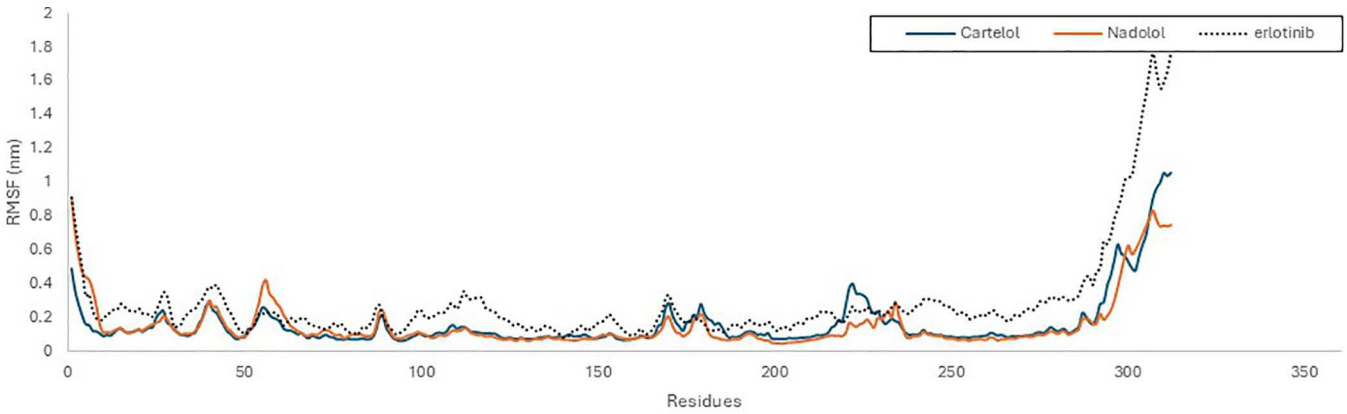


Fig 10. The root means square fluctuation RMSF profile of EGFR (PDB ID: 1M17) with Carteolol (green), Nadolol (orange)and Erlotinib (Black) over a 100 ns simulation time using GROMACs software.

https://doi.org/10.1371/journal.pone.0338123.g010

The radius of gyration (Rg) was utilized as an additional parameter to validate the stability of the protein-ligand complexes as indicated by the RMSD and RMSF findings. Rg measures the distance between the center of mass and the rotational axis of the ligand-protein complex. It represents a measure of the protein structure's compactness and stability throughout the simulation. Lower Rg values indicate greater stability and compactness of the complex, whereas higher values imply reduced stability and compactness. As depicted in Fig 11 the radius of gyration plot for the KRAS ^{G12D} protein illustrates that the three ligands—Carteolol (blue), Nadolol (orange), and MRTX1133 (black)—generally exhibit Rg values ranging from 1.53 to 1.58 nm throughout the simulation, indicating that all complexes maintain a comparable level of compactness. This finding aligned with the results obtained from RMSD and RMSF analyses.

The Radius of Gyration (Rg) plot for the EGFR reveals that both Nadolol and Carteolol induce a more compact conformation compared to Erlotinib, as reflected by their lower Rg values (Fig 12). Although Erlotinib has a lower RMSD than Nadolol and Carteolol, this does not contradict the Rg analysis. The lower RMSD indicates that Erlotinib maintains stable binding interaction, but it may not achieve the same level of compactness as Nadolol and Carteolol.

The ADMET prediction results from the pkCSM server provide important information about the pharmacokinetics and toxicity of the selected compounds (Table 4). Water solubility values (log mol/L) ranged from −2.704 to −3.622, showing

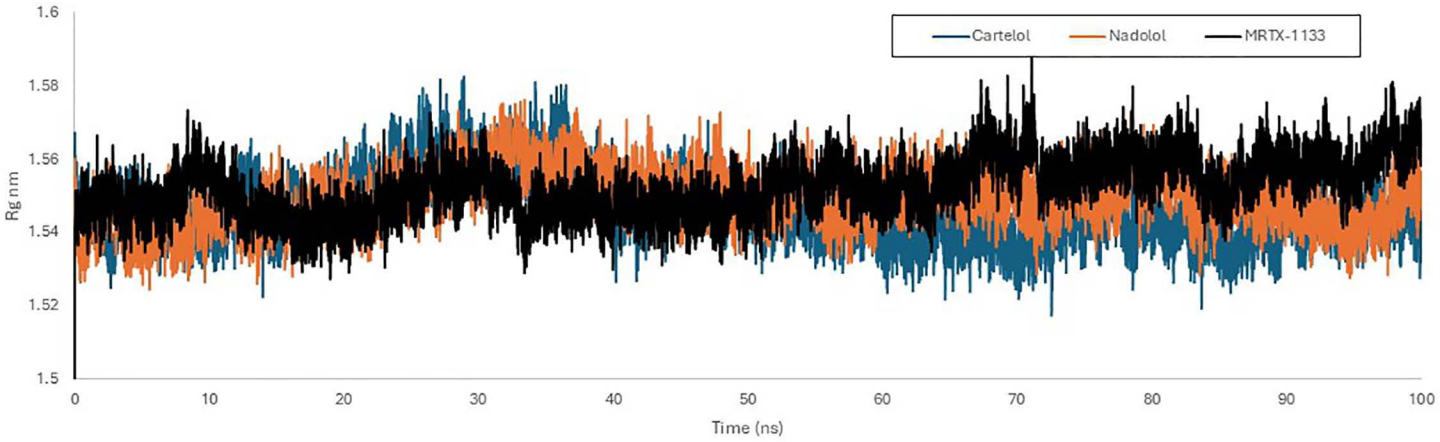


Fig 11. Radius of gyration graph of KRAS $^{G}12^{D}$ (PDB ID: 7RPZ) with Carteolol (Blue), Nadolol (orange) and MRTX1133 (Black) over 100 ns simulation time using GROMACs software.

https://doi.org/10.1371/journal.pone.0338123.g011

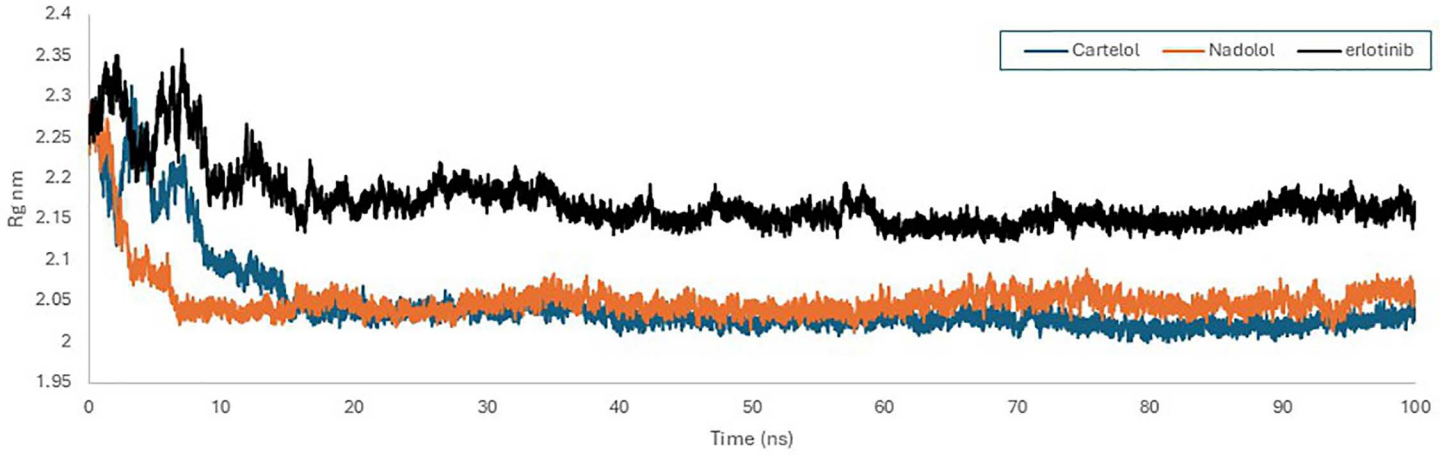


Fig 12. Radius of gyration graph EGFR (PDB ID: 1M17) with Carteolol (Blue), Nadolol (orange)and MRTX1133 (Black) over a 100 ns simulation time using GROMACs software.

https://doi.org/10.1371/journal.pone.0338123.g012

Table 4. The ADMET prediction of the top two drugs and the references.

Compound	Absorption	Distribution	Metabolism						Excretion	Toxicity	
			CYP								
			2D6	3A4	2D6	3A4	1A2	2C9			
	Water solubility	Blood-brain barrier permeability	Substrate		Inhibitor				Renal OCT2 substrate	AMES toxicity	Hepatotoxicity
	Numeric (log mol/L)	Numeric (log BB)	Categorical (Yes/No)						Categorical (Yes/No)	Categorical (Yes/No)	
Nadolol	-2.704	-0.682	No	No	No	No	No	No	No	No	Yes
Carteolol	-3.622	-0.835	Yes	Yes	No	No	No	No	No	No	Yes
MRTX1133	-3.443	-1.62	No	No	No	Yes	Yes	No	No	No	Yes
Erlotinib	-2.892	0.427	No	No	No	No	Yes	No	No	Yes	No

https://doi.org/10.1371/journal.pone.0338123.t004

different solubility levels; Nadolol and Carteolol were less soluble than Erlotinib. Blood-brain barrier permeability (log BB) values indicated that most compounds have limited ability to cross into the brain, with values between −0.682 and −1.62, except Erlotinib, which had a positive value (0.427), suggesting it can penetrate the barrier more easily. This may affect its activity or side effects in the central nervous system. In terms of distribution, Nadolol did not significantly interact with cytochrome P450 enzymes CYP2D6 and CYP3A4, while Carteolol acted as both a substrate and inhibitor of these enzymes, which may influence its metabolism and potential drug interactions.Metabolism predictions showed differences among compounds regarding cytochrome P450 enzyme interactions. MRTX1133 was not a substrate for CYP2D6 or CYP3A4 but inhibited both enzymes, which could affect metabolic pathways. Erlotinib inhibited CYP1A2 but was neither a substrate nor inhibitor of the other tested enzymes. Regarding excretion, none of the compounds were substrates for renal OCT2, affecting their elimination routes. Toxicity predictions indicated Nadolol and Carteolol tested negative for AMES toxicity. All compounds showed hepatotoxicity except Erlotinib.

The findings overall suggest that Carteolol demonstrate notable dual-targeting potential, achieving docking scores of −9.372 kcal/mol for KRAS ^{G12D} and −7.185 kcal/mol for EGFR. Although both interactions were favorable, it displayed stronger binding affinity toward KRAS ^{G12D}. This was further supported by MM-GBSA binding free energy values, with Carteolol exhibiting −57.95 kcal/mol for KRAS ^{G12D} compared to −49.26 kcal/mol for EGFR, reinforcing its preferential binding to the KRAS. Molecular dynamics simulations substantiated these findings by revealing stable and compact interactions with both proteins throughout the simulation period, especially in the KRAS ^{G12D} complex, suggesting robust conformational stability. ADMET prediction showed acceptable properties. The Canvas mean Tanimoto similarity scores using the Canvas's Schrodinger suite indicate very low structural similarity between Nadolol and Carteolol compared to the reference compounds MRTX1133 and Erlotinib. Specifically, Nadolol showed a similarity score of 0.022, while Carteolol had a slightly higher score of 0.036. These values suggest that both Nadolol and Carteolol share minimal chemical features with MRTX1133 and Erlotinib.

Altogether, these results highlight Carteolol's potential as a promising small-molecule agent with preferential affinity for KRAS ^{G12D} and complementary modulation of EGFR, aligning with the study's objective to address resistance mechanisms in colorectal cancer via a dual-targeting strategy. Carteolol is a long-acting, non-selective beta-adrenoceptor antagonist used primarily for the treatment of hypertension. It is also an effective therapy for arrhythmias, angina, and glaucoma. Beyond its cardiovascular applications, beta blockers are gaining recognition in oncology, with both preclinical and clinical studies indicating potential therapeutic benefits outside their conventional use, demonstrating novel mechanisms of action not linked to β-adrenergic receptor blockade. This supports the exploration of new mechanisms that go beyond their traditional roles. Furthermore, β-blockers are suggested to function as immunomodulators. Studies have shown that adrenergic stimulation can enhance cancer hallmarks, such as modulating apoptosis and increasing angiogenesis, effects that beta blockers can counteract. However, the safety profiles of repurposed β-blockers depend on specific conditions and patient characteristics, highlighting the need for further research to optimize their application in non-cardiovascular contexts. Despite these challenges, their potential for treating chronic diseases like cancer positions β-blockers as promising candidates for therapeutic innovation across a broader range of medical fields [11,32,33].

4. Conclusions

This study has employed Insilico tools to identify potential dual-targeting agents for KRAS ^{G12D} and EGFR in colorectal cancer. By screening a library of 3,591 approved drugs through molecular docking, binding free energy calculation and subsequent molecular dynamics simulations, Carteolol emerged as a promising candidate, demonstrating strong binding affinity and stability with both targets. While these computational tools are limited in their capacity to validate biological efficacy fully, they offer a valuable starting point for hypothesis generation and hit identification. Experimental validation via in vitro and in vivo assays is essential to confirm these findings and advance the therapeutic potential of Carteolol in colorectal cancer.

Supporting information

S1. Video. 100 ns molecular dynamics simulation of KRAS ^{G12D} (PDB ID: 7RPZ) with Carteolol (using GROMACs software.
(ZIP)

S1 Table. Prediction of the active site of KRAS using SiteMap.
(DOCX)

S2 Table. Statistics of RMSD of the top two drugs and the references bond to KRAS during 100 ns MD simulation.
(DOCX)

S3 Table. Statistics of RMSD of the top two drugs and the references bond to EGFR during 100 ns MD simulation.
(DOCX)

Acknowledgments

The authors extend their appreciation Mme Katia Dekimeche from Schrodinger for her support and help.

Author contributions

Conceptualization: Walaa Ibraheem.

Data curation: Walaa Ibraheem.

Formal analysis: Walaa Ibraheem, Fatima Alsheikh, Abdulrahim A. Alzain.

Investigation: Walaa Ibraheem, Fatima Alsheikh, Abdulrahim A. Alzain, Laila Ejaz, Hamnah Baig.

Methodology: Walaa Ibraheem, Abdulrahim A. Alzain.

Project administration: Walaa Ibraheem.

Resources: Walaa Ibraheem, Fatima Alsheikh.

Software: Walaa Ibraheem, Fatima Alsheikh.

Supervision: Walaa Ibraheem, Bhoomendra A. Bhongade, Robert C. Robinson, Mohamed El-Tanani.

Validation: Walaa Ibraheem, Fatima Alsheikh.

Visualization: Walaa Ibraheem, Fatima Alsheikh.

Writing – original draft: Walaa Ibraheem.

Writing – review & editing: Walaa Ibraheem, Fatima Alsheikh.

References

1. Ziemke EK, Dosch JS, Maust JD, Shettigar A, Welling TH, Hardiman KM, et al. Sensitivity. Cancer Research. 2017;22:405–14. https://doi.org/10.1158/1078-0432.CCR-15-0829
2. Bannoura SF, Khan HY, Azmi AS. KRAS G12D targeted therapies for pancreatic cancer: Has the fortress been conquered?. Front Oncol. 2022;12:1013902. https://doi.org/10.3389/fonc.2022.1013902 PMID: 36531078
3. Huang L, Guo Z, Wang F, Fu L. KRAS mutation: from undruggable to druggable in cancer. Signal Transduct Target Ther. 2021;6(1):386. https://doi.org/10.1038/s41392-021-00780-4 PMID: 34776511
4. Parikh K, Banna G, Liu SV, Friedlaender A, Desai A, Subbiah V, et al. Drugging KRAS: current perspectives and state-of-art review. J Hematol Oncol. 2022;15(1):152. https://doi.org/10.1186/s13045-022-01375-4 PMID: 36284306
5. Lee T, Kim K, Lee J, Park SH, Park YS, Lim HY, et al. Antitumor activity of sorafenib plus CDK4/6 inhibitor in pancreatic patient derived cell with KRAS mutation. J Cancer. 2018;9(18):3394–9. https://doi.org/10.7150/jca.26068 PMID: 30271501
6. Hofmann MH, Gerlach D, Misale S, Petronczki M, Kraut N. Expanding the Reach of Precision Oncology by Drugging All KRAS Mutants. Cancer Discov. 2022;12(4):924–37. https://doi.org/10.1158/2159-8290.CD-21-1331 PMID: 35046095

7. Wei D, Wang L, Zuo X, Maitra A, Bresalier RS. A Small Molecule with Big Impact: MRTX1133 Targets the KRASG12D Mutation in Pancreatic Cancer. Clin Cancer Res. 2024;30(4):655–62. https://doi.org/10.1158/1078-0432.CCR-23-2098 PMID: 37831007
8. Wang X, Allen S, Blake JF, Bowcut V, Briere DM, Calinisan A, et al. Identification of MRTX1133, a noncovalent, potent, and selective KRAS. 2022.
9. Wang X, Allen S, Blake JF, Bowcut V, Briere DM, Calinisan A, et al. Identification of MRTX1133, a Noncovalent, Potent, and Selective KRASG12D Inhibitor. J Med Chem. 2022;65(4):3123–33. https://doi.org/10.1021/acs.jmedchem.1c01688 PMID: 34889605
10. Feng J, Hu Z, Xia X, Liu X, Lian Z, Wang H, et al. Feedback activation of EGFR/wild-type RAS signaling axis limits KRASG12D inhibitor efficacy in KRASG12D-mutated colorectal cancer. Oncogene. 2023;42(20):1620–33. https://doi.org/10.1038/s41388-023-02676-9 PMID: 37020035
11. Malik JA, Ahmed S, Momin SS, Shaikh S, Alafnan A, Alanazi J, et al. Drug Repurposing: A New Hope in Drug Discovery for Prostate Cancer. ACS Omega. 2022;8(1):56–73. https://doi.org/10.1021/acsomega.2c05821 PMID: 36643505
12. Ahamad S, Hema K, Gupta D. Structural stability predictions and molecular dynamics simulations of RBD and HR1 mutations associated with SARS-CoV-2 spike glycoprotein. J Biomol Struct Dyn. 2022;40(15):6697–709. https://doi.org/10.1080/07391102.2021.1889671 PMID: 33618621
13. Ahamad S, Hema K, Ahmad S, Kumar V, Gupta D. Insights into the structure and dynamics of SARS-CoV-2 spike glycoprotein double mutant L452R-E484Q. 3 Biotech. 2022;12(4):87. https://doi.org/10.1007/s13205-022-03151-0 PMID: 35265451
14. Borse PBN, Konwar VAN. Screening malaria-box compounds to identify potential inhibitors against SARS-CoV-2 Mpro, using molecular docking and dynamics simulation studies. Psychiatry Res. 2020;14(4):293.
15. Yadav S, Ahamad S, Gupta D, Mathur P. Lead optimization, pharmacophore development and scaffold design of protein kinase CK2 inhibitors as potential COVID-19 therapeutics. J Biomol Struct Dyn. 2023;41(5):1811–27. https://doi.org/10.1080/07391102.2021.2024449 PMID: 35014595
16. Sastry GM, Adzhigirey M, Day T, Annabhimoju R, Sherman W. Protein and ligand preparation: parameters, protocols, and influence on virtual screening enrichments. J Comput Aided Mol Des. 2013;27(3):221–34. https://doi.org/10.1007/s10822-013-9644-8 PMID: 23579614
17. Ali AM, Makki AA, Ibraheem W, Abdelrahman M, Osman W, Sherif AE, et al. Design of Novel Phosphatidylinositol 3-Kinase Inhibitors for Non-Hodgkin's Lymphoma: Molecular Docking, Molecular Dynamics, and Density Functional Theory Studies on Gold Nanoparticles. Molecules. 2023;28(5):2289. https://doi.org/10.3390/molecules28052289 PMID: 36903539
18. Yousif FA, Alzain AA, Alraih AM, Ibraheem W. Repurposing of approved drugs for targeting CDK4/6 and aromatase protein using molecular docking and molecular dynamics studies. PLoS One. 2023;18(9):e0291256. https://doi.org/10.1371/journal.pone.0291256 PMID: 37682937
19. AbdElmoniem N, H Abdallah M, M Mukhtar R, Moutasim F, Rafie Ahmed A, Edris A, et al. Identification of Novel Natural Dual HDAC and Hsp90 Inhibitors for Metastatic TNBC Using e-Pharmacophore Modeling, Molecular Docking, and Molecular Dynamics Studies. Molecules. 2023;28(4):1771. https://doi.org/10.3390/molecules28041771 PMID: 36838758
20. Friesner RA, Banks JL, Murphy RB, Halgren TA, Klicic JJ, Mainz DT, et al. Glide: a new approach for rapid, accurate docking and scoring. 1. Method and assessment of docking accuracy. J Med Chem. 2004;47(7):1739–49. https://doi.org/10.1021/jm0306430 PMID: 15027865
21. Friesner RA, Murphy RB, Repasky MP, Frye LL, Greenwood JR, Halgren TA, et al. Extra precision glide: docking and scoring incorporating a model of hydrophobic enclosure for protein-ligand complexes. J Med Chem. 2006;49(21):6177–96. https://doi.org/10.1021/jm051256o PMID: 17034125
22. Halgren TA, Murphy RB, Friesner RA, Beard HS, Frye LL, Pollard WT, et al. Glide: a new approach for rapid, accurate docking and scoring. 2. Enrichment factors in database screening. J Med Chem. 2004;47(7):1750–9. https://doi.org/10.1021/jm030644s PMID: 15027866
23. Maffucci I, Hu X, Fumagalli V, Contini A. An Efficient Implementation of the Nwat-MMGBSA Method to Rescore Docking Results in Medium-Throughput Virtual Screenings. Front Chem. 2018;6:43. https://doi.org/10.3389/fchem.2018.00043 PMID: 29556494
24. Genheden S, Ryde U. The MM/PBSA and MM/GBSA methods to estimate ligand-binding affinities. Expert Opin Drug Discov. 2015;10(5):449–61. https://doi.org/10.1517/17460441.2015.1032936 PMID: 25835573
25. Fang W-S, Zhang J. Natural products. Curr Top Med Chem. 2009;9(17):1597. https://doi.org/10.2174/156802609789941942 PMID: 19939219
26. Heinzelmann G, Gilson MK. Automation of absolute protein-ligand binding free energy calculations for docking refinement and compound evaluation. Sci Rep. 2021;11(1):1116. https://doi.org/10.1038/s41598-020-80769-1 PMID: 33441879
27. Zoete V, Cuendet MA, Grosdidier A, Michielin O. SwissParam: a fast force field generation tool for small organic molecules. J Comput Chem. 2011;32(11):2359–68. https://doi.org/10.1002/jcc.21816 PMID: 21541964
28. Zou J, Shi X, Wu Z, Zuo S, Tang X, Zhou H, et al. MRTX1133 attenuates KRASG12D mutated-colorectal cancer progression through activating ferroptosis activity via METTL14/LINC02159/FOXC2 axis. Transl Oncol. 2025;52:102235. https://doi.org/10.1016/j.tranon.2024.102235 PMID: 39657309
29. Issahaku AR, Mukelabai N, Agoni C, Rudrapal M, Aldosari SM, Almalki SG, et al. Characterization of the binding of MRTX1133 as an avenue for the discovery of potential KRASG12D inhibitors for cancer therapy. Sci Rep. 2022;12(1):17796. https://doi.org/10.1038/s41598-022-22668-1 PMID: 36273239
30. Peng Y-H, Shiao H-Y, Tu C-H, Liu P-M, Hsu JT-A, Amancha PK, et al. Protein kinase inhibitor design by targeting the Asp-Phe-Gly (DFG) motif: the role of the DFG motif in the design of epidermal growth factor receptor inhibitors. J Med Chem. 2013;56(10):3889–903. https://doi.org/10.1021/jm400072p PMID: 23611691
31. De Vivo M, Masetti M, Bottegoni G, Cavalli A. Role of Molecular Dynamics and Related Methods in Drug Discovery. J Med Chem. 2016;59(9):4035–61. https://doi.org/10.1021/acs.jmedchem.5b01684 PMID: 26807648
32. Shahid A, Wang J, Andresen BT, Chen SRW, Huang Y. Editorial: Repurposing β-blockers for non-cardiovascular diseases. Front Pharmacol. 2024;15:1372317. https://doi.org/10.3389/fphar.2024.1372317 PMID: 38405668
33. Benjamin DJ, Haslam A, Prasad V. Cardiovascular/anti-inflammatory drugs repurposed for treating or preventing cancer: A systematic review and meta-analysis of randomized trials. Cancer Med. 2024;13(5):e7049. https://doi.org/10.1002/cam4.7049 PMID: 38491813